

Article

Skeletal Torsion Tunneling and Methyl Internal Rotation: The Coupled Large Amplitude Motions in Phenyl Acetate

Lynn Ferres ¹, Luca Evangelisti ² , Assimo Maris ² , Sonia Melandri ² , Walther Caminati ^{2,*}, Wolfgang Stahl ^{1,†} and Ha Vinh Lam Nguyen ^{3,4,*} 

¹ Institute of Physical Chemistry, RWTH Aachen University, Landoltweg 2, D-52074 Aachen, Germany; lynn.ferres@rwth-aachen.de

² Dipartimento di Chimica “G. Ciamician”, Università di Bologna, Via Selmi 2, 40126 Bologna, Italy; luca.evangelisti6@unibo.it (L.E.); assimo.maris@unibo.it (A.M.); sonia.melandri@unibo.it (S.M.)

³ Univ Paris Est Creteil and Université Paris Cité, CNRS, LISA, F-94010 Créteil, France

⁴ Institut Universitaire de France (IUF), F-75231 Paris, France

* Correspondence: walther.caminati@unibo.it (W.C.); lam.nguyen@lisa.ipsl.fr (H.V.L.N.)

† Deceased.

Abstract: The rotational spectrum of phenyl acetate, CH₃COOC₆H₅, is measured using a free jet absorption millimeter-wave spectrometer in the range from 60 to 78 GHz and two pulsed jet Fourier transform microwave spectrometers covering a total frequency range from 2 to 26.5 GHz. The features of two large amplitude motions, the methyl group internal rotation and the skeletal torsion of the CH₃COO group with respect to the phenyl ring C₆H₅ (tilted at about 70°), characterize the spectrum. The vibrational ground state is split into four widely spaced sublevels, labeled as A₀, E₀, A₁, and E₁, each of them with its set of rotational transitions and with additional interstate transitions. A global fit of the line frequencies of the four sublevels leads to the determination of 51 spectroscopic parameters, including the $\Delta E_{A_0/A_1}$ and $\Delta E_{E_0/E_1}$ vibrational splittings of ~36.4 and ~33.5 GHz, respectively. The V_3 barrier to methyl internal rotation (~136 cm⁻¹) and the skeletal torsion B_2 barrier to the orthogonality of the two planes (~68 cm⁻¹) are deduced.

Keywords: internal rotation; large amplitude motions; skeletal motion tunneling; rotational spectroscopy



Citation: Ferres, L.; Evangelisti, L.; Maris, A.; Melandri, S.; Caminati, W.; Stahl, W.; Nguyen, H.V.L. Skeletal Torsion Tunneling and Methyl Internal Rotation: The Coupled Large Amplitude Motions in Phenyl Acetate. *Molecules* **2022**, *27*, 2730. <https://doi.org/10.3390/molecules27092730>

Academic Editor: Jan Sýkora

Received: 27 March 2022

Accepted: 19 April 2022

Published: 23 April 2022

Publisher’s Note: MDPI stays neutral with regard to jurisdictional claims in published maps and institutional affiliations.



Copyright: © 2022 by the authors. Licensee MDPI, Basel, Switzerland. This article is an open access article distributed under the terms and conditions of the Creative Commons Attribution (CC BY) license (<https://creativecommons.org/licenses/by/4.0/>).

1. Introduction

Phenyl acetate (CH₃COOC₆H₅, also called phenyl ethanoate, phenol acetate, acetyloxybenzene, or acetoxybenzene) is a colorless liquid with a plastic-like odor, often used as a solvent in chemical reactions. It can be synthesized by adding acetic anhydride to phenol [1], via Baeyer–Villiger oxidation of acetophenone [2], or by decarboxylation of aspirin [3]. Currently, phenyl acetate is a drug being studied in the treatment of cancer [4]. Naturally occurring in mammals, phenyl acetate induces differentiation, growth inhibition, and apoptosis in tumor cells. Despite the great interest in medicine, knowledge of its molecular structure is very limited, though it might be helpful to develop force fields to study biological processes at a molecular scale towards understanding how phenyl acetate affects tumor cells.

Many acetates have already been studied using rotational spectroscopy, notably a series of linear aliphatic acetates starting from methyl acetate to hexyl acetate [5–10]. The methyl group in the acetyl moiety undergoes internal rotation, causing each rotational transition to split into an A-E doublet. The torsional barrier is almost invariant at approximately 100 cm⁻¹ [7]. If a C=C double bond is attached at the α,β -position counting after the oxygen atom, the value increases to about 150 cm⁻¹, as in the case of vinyl acetate [11,12] and butadienyl acetate [13] where the double bond(s) are located in the OCO-plane. Surprisingly, this is not the case in isopropenyl acetate, where we observed an unusual C₁ structure. The isopropenyl group is tilted out of the OCO-plane, and a torsional barrier of 135.3498(38)

cm^{-1} was deduced, a value which lies between 100 and 150 cm^{-1} [14]. Since the molecular structure of phenyl acetate is very similar to that of isopropenyl acetate, we were interested in answering two questions: (i) Does phenyl acetate have a C_s or C_1 symmetry? (ii) How high is the barrier to internal rotation of the methyl group of phenyl acetate?

Though in many cases, studies on medium-sized molecules containing a phenyl ring have reported a planar heavy-atom structure as the most stable one, such as anisole [15], phenetole [16], methyl salicylate [17], or acetophenone [18], there are several molecules where at least one conformer observed in the rotational spectrum has C_1 symmetry. For example, the CH_2OH group in benzyl alcohol [19] as well as in its derivative 3,5-difluorobenzyl alcohol [20] is tilted out of the phenyl ring. In the case of 2-phenylethylamine, none of the observed four conformers possesses a structure where all heavy atoms are within the aromatic plane [21,22]. In *cis*-acetanilide, $\text{C}_6\text{H}_5(\text{NH})(\text{CO})\text{CH}_3$, Cabezas et al. reported doublets with splittings in the order of a few tens of kHz [23]. They were interpreted to be due to the tunneling motion of the phenyl ring between two equivalent non-planar conformations, with the phenyl ring tilted out of the $(\text{NH})(\text{CO})$ plane by about 40° through a transition state where the acetamide group and the phenyl ring are perpendicular. Aviles Moreno, Petitprez, and Huet observed similar splittings in the order of about 100 kHz for *E*-phenylformamide, where the phenyl ring is tilted out of the $(\text{NH})(\text{CO})$ plane by the same angle [24]. These splittings arise from Coriolis interactions, from which the ΔE_{01} value was determined to be $3.732027(43)$ GHz. In phenyl formate [25], the phenyl ring tilt angle of 72° is remarkably larger than in *cis*-acetanilide and *E*-phenylformamide, and the ring also undergoes a tunneling large amplitude motion (LAM). The energy levels of molecules featuring such an inversion motion split into a (+) and a (−) state due to a symmetric and an anti-symmetric wave function, separated by ΔE_{01} , for example in ammonia [26] (see Figure 1) [27]. In phenyl formate, the ΔE_{01} value of $46.2231(25)$ GHz is large, making the $(+)\leftarrow(-)$ and $(-)\leftarrow(+)$ transitions non-observable in the frequency range accessible by the spectrometer in use. However, the theoretically unsplit $(\pm)\leftarrow(\pm)$ transitions still show small splittings, referred to as $v_t = 0$ and $v_t = 1$, due to Coriolis interactions, which were observed and could be fitted with the *spfit* program [28], but many complications occurred in further assignments and fitting processes that relied on a small number of the less intense $v_t = 1$ transitions and Coriolis splittings between the $v_t = 0$ and 1 states.

Regarding the closely related forms of phenyl acetate and phenyl formate, we supposed a similar structure with the phenyl ring and the $\text{O}(\text{C}=\text{O})\text{C}$ plane tilted with respect to each other, enabling a skeletal tunneling motion. However, phenyl acetate features an additional methyl internal rotor, which further splits the rotational signals into an A and an E symmetry species. Thus, the A-E pairs are expected for each transition of the torsional levels, resulting in a total of four species called A0, E0 ($v_t = 0$), and A1, E1 ($v_t = 1$). Note that these sublevels could be labeled more properly as A^+ , A^- , E^+ , and E^- . The splittings are shown in the energy level scheme in Figure 1. To fit transition frequencies belonging to different phenyl tunneling states, the *spfit* program is well-suited. Some of its main advantages are the possibility for users to build up an individual Hamiltonian, the ability to define any desired parameters in the input, and the short calculation time. Unfortunately, *spfit* can only fit the A and E torsional transitions separately, and deriving the torsional barrier is a tedious task in low barrier cases [29]. The program XIAM is a counterpart, which is specialized for fitting the A-E splittings due to three-fold methyl internal rotation but is incapable of treating tunneling states arising from a two-fold potential [30]. A further separate fit was performed with the XIAM program where only the A0–E0 doublets are considered to alternatively access the methyl torsional barrier.

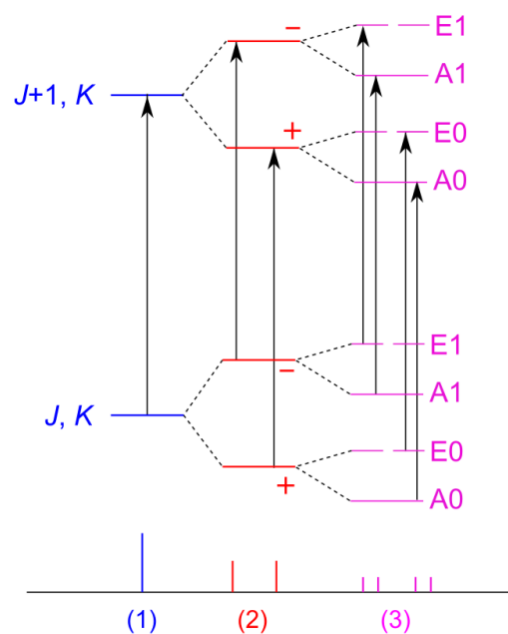


Figure 1. Non-scaled energy levels and microwave signal splittings for different types of molecules. (1) Asymmetric rigid rotor (e.g., phenetole [16]), (2) One two-fold tunneling motion (e.g., phenyl formate with the tunneling of the phenyl ring [25]), (3) One two-fold tunneling motion and a methyl internal rotation (e.g., phenyl acetate with the tunneling of the phenyl ring and the internal rotation of the acetyl methyl group, this work). Rotational a -type transitions are indicated as black arrows. Please note that, for sake of simplicity, the symmetric top J, K label is used to indicate the rotational levels, rather than the correct J, K_a, K_c one.

2. Results

2.1. Quantum Chemical Calculations

Using the *Gaussian 16* program package [31], the molecular structure of phenyl acetate was optimized at the MP2/6-311G++(d,p) level of theory, revealing a non-planar structure with the methyl group *entgegen* with respect to the phenyl ring, called conformer I, illustrated in Figure 2. A second conformer, with the methyl group *zusammen* with respect to the ring, was calculated much higher in energy (1347 cm^{-1}) and was not considered in the present work. Similar to the case of phenyl formate, the phenyl ring is tilted out of the O-(C=O)-C plane by about 72° for conformer I. Due to the symmetry of the phenyl ring and the planarity of the acetyl moiety, four equivalent minima are possible, as shown in Figure 3, where the dihedral angle $\alpha = \angle(\text{C}_{13}\text{-O}_{12}\text{-C}_3\text{-C}_2)$ was varied in 10° steps, while all other geometry parameters were optimized. The obtained energy points were parametrized using a Fourier expansion, including terms with the correct symmetry of α , which are collected in Table S1 in the Supplementary Materials. The two pairs I_a/I_a^* and I_b/I_b^* describe two double minima in the potential energy curve, separated by a barrier of 20.65 cm^{-1} , while I_a and I_b , as well as I_a^* and I_b^* , can be converted into each other by rotating the phenyl ring by 180° with a much higher conversion barrier of 837.45 cm^{-1} . The geometry of the local maximum between I_a and I_a^* (or I_b and I_b^*) was also optimized as a transition state, yielding a slightly higher barrier of 26.71 cm^{-1} . The dihedral angle $\beta = \angle(\text{C}_3\text{-O}_{12}\text{-C}_{13}\text{-C}_{14})$ corresponds to the orientation of the acetyl group and stays nearly invariant at 180° in the *entgegen* configuration, which is known to be much more stable than the *zusammen* one ($\beta = 0^\circ$). The Cartesian coordinates of the I_b structure are given in Table S2 in the Supplementary Materials. The rotational constants are $A = 3592.4315\text{ MHz}$, $B = 813.8922\text{ MHz}$, and $C = 744.3161\text{ MHz}$; the three dipole moment components are $\mu_a = -0.41\text{ D}$, $\mu_b = 0.90\text{ D}$, and $\mu_c = -1.46\text{ D}$. Therefore, mainly b - and c -type transitions are expected in the rotational spectrum, eventually accompanied by some weak a -type signals. Frequency calculations were carried out at the same level of theory, yielding an imaginary frequency describing a

ring bending motion. This observation has been frequently reported in calculations using the MP2 method [32]. Repeating the geometry optimization and frequency calculations at various levels of theory shows that most levels state no imaginary frequency.

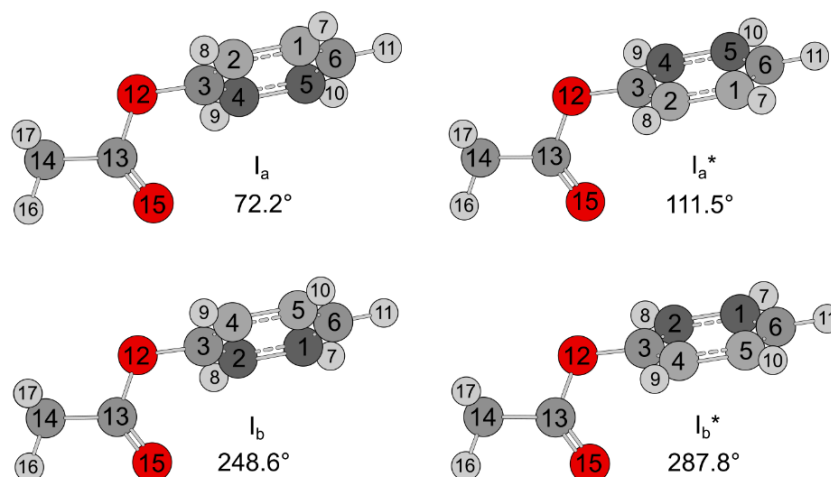


Figure 2. Four minima equivalent in energy at $E = -458.9579885 E_h$ of the most stable conformer I (*entgegen*) of phenyl acetate with C_1 -symmetry. The geometries were fully optimized at the MP2/6-311++G(d,p) level of theory. The dihedral angle $\beta = \angle(C_3-O_{12}-C_{13}-C_{14})$ describes the *entgegen* orientation of the acetyl group and is 180° , while $\alpha = \angle(C_{13}-O_{12}-C_3-C_2)$ corresponds to the orientation of the phenyl ring, which is 72.2° for I_a , 111.5° for I_a^* , 248.6° for I_b , and 287.8° for I_b^* . Note that $\alpha \approx 90^\circ$ or 270° at the transition states, corresponding to a tunneling angle of about 40° from one minimum to the other.

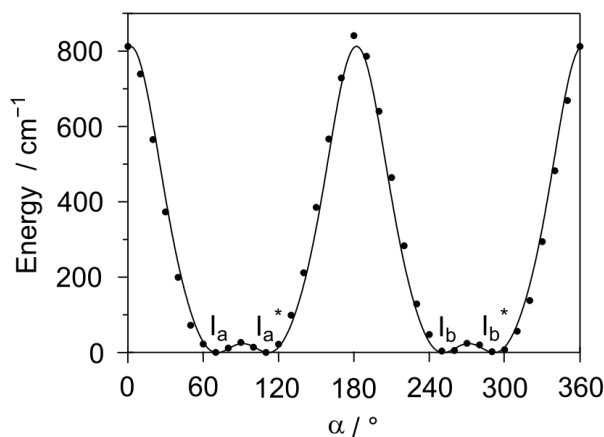


Figure 3. Potential energy curve of phenyl acetate obtained by varying the dihedral angle $\alpha = \angle(C_{13}-O_{12}-C_3-C_2)$ in 10° steps. The two double minima correspond to the I_a/I_a^* and I_b/I_b^* pairs. The barrier to convert I_a in I_a^* or I_b in I_b^* is 20.65 cm^{-1} ; that to convert I_a in I_b or I_a^* in I_b^* is 837.45 cm^{-1} . The minima are at $\alpha = 70^\circ, 110^\circ, 250^\circ,$ and 290° with an energy of $E = -458.9579885 E_h$. All other energy values are relative to this value.

The dihedral angle $\gamma = \angle(O_{15}-C_{13}-C_{14}-H_{16})$ was varied in a 10° grid to calculate the torsional barrier of the methyl internal rotation. The potential curve is given in Figure 4. From the Fourier parameterization (see Table S1 in the Supplementary Materials), we determined a V_3 term of 113.18 cm^{-1} . A very similar value of 113.40 cm^{-1} was deduced by optimizing the maxima as transition states [33].

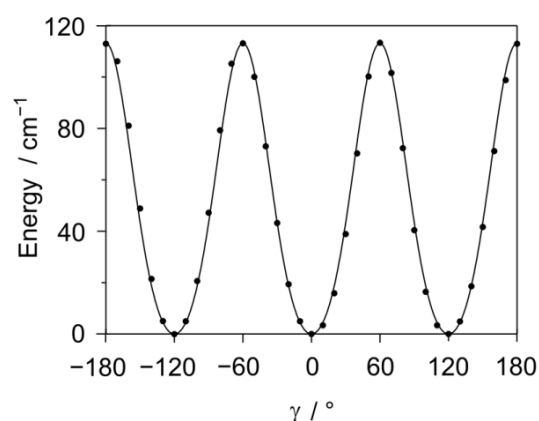


Figure 4. The threefold potential obtained by rotating the methyl group about the C_{13} - C_{14} axis (variation of the dihedral angle $\gamma = \angle(O_{15}-C_{13}-C_{14}-H_{16})$). The optimized structure of conformer I_a served as the input structure. Three equivalent minima were obtained for $\gamma = -120^\circ, 0^\circ,$ and 120° . The torsional barrier of about 113 cm^{-1} is relatively low, suggesting large torsional splittings in the microwave spectrum. Energies are given relative to $E_{\min} = -458.9577608 E_h$.

To study the coupling between the two LAMs, we calculated a two-dimensional potential energy surface (2D-PES) depending on α and γ , as shown in Figure 5. The obtained energy points were also parameterized using a Fourier expansion, including terms with the correct symmetry of α and γ given in Table S3 in the Supplementary Materials. Along the γ -axis, the threefold symmetry of the methyl group can be clearly seen. For a given γ minimum, for example, $\gamma = 0^\circ$, the four equivalent structures along the α -axis are also recognizable. The minima regions of this 2D-PES are very broad and flat. Therefore, more colors were used in the lower 50% area to enable the distinction of the four minima.

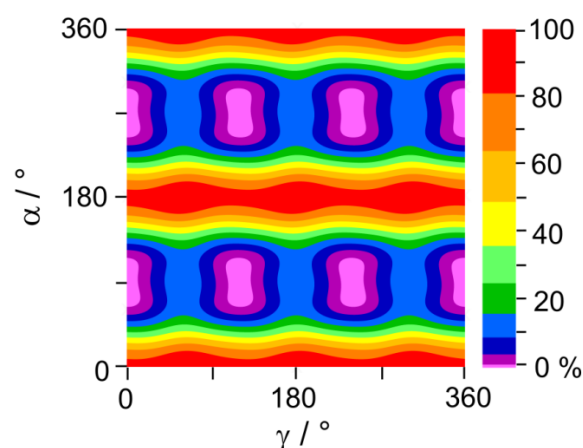


Figure 5. The potential energy surface of phenyl acetate calculated at the MP2/6-311++G(d,p) level of theory in dependence of the dihedral angles α and γ . The energies are given in percentage color code, relative to $E_{\min} = -458.9579660 E_h$ (0%), and $E_{\max} = -458.9533836 E_h$ (100%). The relative energy of the maximum is about 12 kJ/mol. Note that there are more colors in the lower 50% region.

At this point, it is clear that the situation observed for phenyl acetate is very similar, for the skeletal torsion, to that of phenyl formate [25]. The tunneling LAM of the skeletal motion causes low-lying excited torsional states, which are most probably observable in the rotational spectrum. To calculate these tunneling states, a two-rigid-top model was applied, as described in Ref. [25], using the following Hamiltonian:

$$H = -F \frac{d^2}{d\alpha^2} + V_0 + \sum_{n=1}^7 V_{2n} \cos(2n\alpha). \quad (1)$$

The effective torsional constant F of 0.32635 cm^{-1} is calculated as $h/8\pi^2 Ic$, where $I = 51.654 \text{ u}\text{\AA}^2$ is the effective moment of inertia and c is the speed of light. I is calculated from the moments of inertia of the phenyl top $I_p = 121.034 \text{ u}\text{\AA}^2$ and of the acetyl top $I_{ac} = 90.112 \text{ u}\text{\AA}^2$. Both were taken from ab initio. The Fourier expansion terms are those obtained from the parameterization of the potential energy curve given in Figure 3. Direct diagonalization of the built-up Hamiltonian matrix yields the following eigenvalues, which represent the energies of the degenerate torsional states given in parentheses: 13.801 (0), 14.823 (1), 31.931 (2), and 42.330 (3) cm^{-1} . The potential function in the range from 50° to 130° , including the torsional energy states, is illustrated in Figure 6.

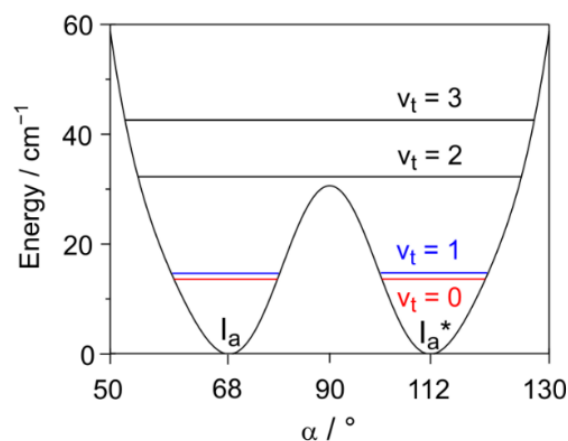


Figure 6. An enlarged portion from 50° to 130° of the potential energy curve given in Figure 3. The doubly degenerate lowest tunneling energy levels $v_t = 0, 1, 2, 3$ are indicated by horizontal lines.

The difference between the first two levels, $v_t = 0$ and 1 , is only 1.022 cm^{-1} , corresponding to 30.64 GHz , which is the value of ΔE_{01} . Calculating the Boltzmann distribution yields an N_1/N_0 ratio of 0.23 to 0.48 for a temperature of 1 to 2 K , i.e., the population of the first excited state $v_t = 1$ is expected to be 23 to 48% with respect to the ground state $v_t = 0$.

2.2. Rotational Spectroscopy

2.2.1. Experimental Setups

The rotational spectrum was first observed using the Bologna free jet absorption millimeter-wave spectrometer in the range from 60 to 78 GHz [34–36]. Initially, families of intrastate ($v_t = 0, 1$) μ_c -R-type transitions such as $J_{10,x} \leftarrow (J-1)_{9,x}$ and $J_{9,y} \leftarrow (J-1)_{8,y}$ (with J up to 18) were measured and fitted, followed by many intrastate μ_a -R-type transitions and several (unexpected, because only μ_b is inverting) interstate μ_a -R-type transitions (see the explanation in a following section) [37]. The estimated uncertainty for the measurements is about 50 kHz . The sample was heated to 65 – 70°C while a stream of argon with a backing pressure of $P_a = 18 \text{ kPa}$ flowed over it. The mixture was then expanded to about $P_b = 0.5 \text{ Pa}$ through a 0.3 mm diameter pinhole nozzle. The estimated rotational temperature of the molecules in the jet is 5 – 10 K . Later on, extensive measurements were made with two molecular jet Fourier transform microwave (MJ-FTMW) spectrometers, one in Bologna [38] (the assignment of the E0 state was made in a way similar to that described in the next section for Aachen) and one in Aachen [39]. Using the scan mode (50 co-added free induction decays per each step in a 250 kHz step width), a broadband scan was recorded from 8 to 14 GHz with the Aachen MJ-FTMW spectrometer. The substance, with a stated purity of 99% , was purchased from Sigma Aldrich, Taufkirchen, Germany, and was used without further purification. Under helium-stream, the phenyl acetate—He mixture entered the vacuum chamber under a backing pressure of 200 Pa . All signals appeared as doublets due to the Doppler effect and were re-measured with higher resolution and under an increased number of free induction decays. The measurement accuracy of both MJ-FTMW

spectrometers is about 2 kHz [40]. Eventually, line broadening occurred as a result of unresolved splittings arising from proton hyperfine structures or spin-couplings.

2.2.2. Assignment of the $v_t = 0$, A Species (A0)

Using a rigid rotor model with the values for the rotational constants calculated at the MP2/6-311++G(d,p) level, the R-branch $J+1_J \leftarrow J_0J$ and the Q-branch $J_{2,J-2} \leftarrow J_{1J}$ with $J \leq 5$ were assigned from the survey scan recorded with the Aachen MJ-FTMW spectrometer, independently from the assignment in the millimeter-wave range. The first fit attempts using only three rotational constants yielded a root-mean-squares (rms) deviation of 1.7 MHz. After more lines with higher J and K_a from the scan were included in a fit containing 20 lines, five centrifugal distortion constants could be floated, and the rms deviation decreased to 1.24 MHz, which is still extremely large compared to the experimental accuracy of 2 kHz of the MJ-FTMW spectrometer. However, when simulating the spectrum with the fitted rotational and centrifugal distortion constants and comparing it to the measured spectrum, as shown in Figure 7, we were confident that the assignment was correct. Using predictions with the fitted parameters, we found some more lines outside the 8–14 GHz scan area and achieved a fit with 36 lines and an rms deviation of 1.3 MHz.

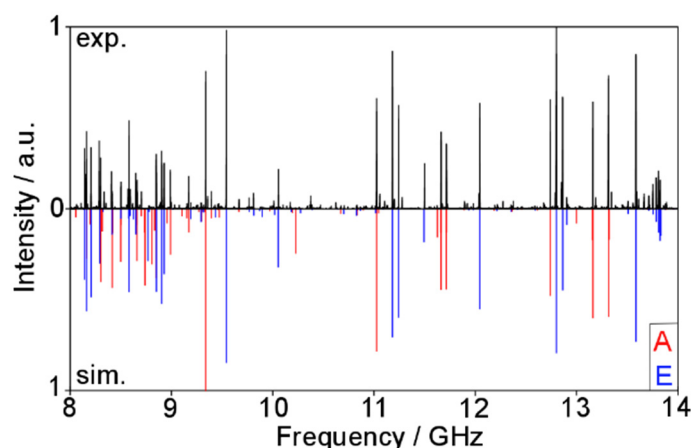


Figure 7. Upper trace: The recorded survey spectrum of phenyl acetate reaching from 8 to 14 GHz. Lower trace: The theoretical spectrum reproduced with the parameters obtained from Fit A0/E0 (see text). The A0 species transitions are marked in red, the E0 species in blue.

This struggle in fitting a species using a rigid rotor model supplemented by centrifugal distortion corrections is extremely similar to the fitting procedure in pinacolone [41] and phenyl formate [25]. As the double minimum potential suggests a strong Coriolis coupling in phenyl acetate, a new fit was carried out using the *spfit* program, which can implement Coriolis cross terms. Adding E (corresponding to ΔE_{01}), E_J (multiplying J^2), F_{bc} (multiplying $J_b J_c + J_c J_b$), and F_{ab} (multiplying $J_a J_b + J_b J_a$) in the fit, the rms decreased to 1.7 kHz, and a total of 80 $v_t = 0$, A species (A0) lines could be assigned in the microwave range. In addition, the assignments of the microwave lines were secured with extensive interlocking combination difference loops, as illustrated in Figure 8. The fit is shown as Fit A0 in Table S4 of the Supplementary Materials with a list of all fitted frequencies along with their residuals.

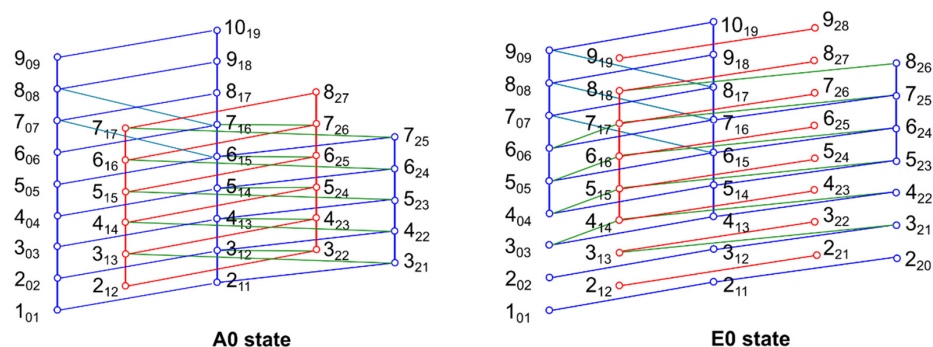


Figure 8. Schematic illustration of some rotational energy levels $J_{K_a K_c}$ (open circles) of the A0 and E0 species of phenyl acetate measured with the Aachen FTMW spectrometer. Solid lines connecting the circles indicate transitions that are checked by combination difference loops, which sum to values in good agreement with the expected measurement uncertainty of 2 kHz. These transitions were used for an initial *spfit* fit whose *spcat* predictions have guided the assignments of further lines. Note that for the E0 states, some *a*-type transitions are weak or fall in resonance ranges of the spectrometer and could not be measured. Therefore, some loops are not closed.

2.2.3. Assignment of the $v_t = 1$, A Species (A1)

After the A0 species was assigned, we found a series of satellite lines close to the strongest A0 species lines. From our experiences with the microwave spectrum of phenyl formate [25], we suspected these transitions to be those of the $v_t = 1$, A species (A1). In a second step, 20 A1 lines could be identified and included in a fit where the rotational and centrifugal distortion constants were fitted separately for the $v_t = 0$ and 1 states (Fit A0/A1 MW in Table S4). The rms deviation only increased slightly to 3.6 kHz. The effective Hamiltonian:

$$H = \sum_{v=0}^1 \langle v | (H_r^v + H_\Delta^v) \quad (2)$$

was applied where $0\rangle$ and $1\rangle$ represent the symmetric and the anti-symmetric torsional states, respectively, unifying the following operators that describe:

- (i) the overall rotation including quartic centrifugal distortion constants:

$$H_r^v = A_v J_a^2 + B_v J_b^2 + C_v J_c^2 - D_{J,v} J^4 - D_{JK,1} J^2 J_a^2 - D_{K,1} J_a^4 + d_{1,1} J^2 (J_+^2 \mp J_-^2) + d_{2,0} (J_+^4 + J_-^4) \quad (3)$$

- (ii) the torsional splitting between the $0\rangle$ and the $1\rangle$ energy levels:

$$H_\Delta^v = vE \quad (4)$$

- (iii) and the Coriolis interaction:

$$H_c = F_{ab} (J_a J_b + J_b J_a) + F_{ab} J^2 (J_a J_b + J_b J_a) + F_{bc} (J_b J_c + J_c J_b) + F_{bc} J^2 (J_b J_c + J_c J_b) \quad (5)$$

The A0/A1 measurements in the microwave range with significantly fewer $v_t = 1$ lines compared to the number of $v_t = 0$ lines were then combined with those in the millimeter-wave range from 60 to 78 GHz, where 40 lines were observed, almost equally distributed between the $v_t = 0$ and 1 states. We could also assign 26 *a*-type interstate transitions $v_t = 0 \leftarrow 1$ or $1 \leftarrow 0$ (note that some of them are blended). The fit is shown as Fit A0/A1 MW+mmw in Table S4 of the Supplementary Materials.

2.2.4. Assignment of the $v_t = 0$, E Species (E0)

Assigning the E0 state was a tedious task because the *spfit*/*spcat* program suite was not useful at the initial stage for assigning the internal rotation E species lines and the XIAM program could not deal with the tunneling motion of the phenyl ring. We first used XIAM to predict a theoretical microwave spectrum for the scan region (8–14 GHz) with

the rotational constants of Fit A0 given in Table S4 of the Supplementary Materials, the V_3 potential term, and the angles between the internal rotor axis and the principal axes of inertia obtained from calculations at the MP2/6-311++G(d,p) level. The most intense b - and c -type $J'_{K'_a K'_c} \leftarrow J_{K_a K_c} = 4_{13} \leftarrow 3_{03}, 5_{14} \leftarrow 4_{04}, 6_{16} \leftarrow 5_{05}, 2_{20} \leftarrow 1_{10}, 3_{21} \leftarrow 2_{11}, 2_{21} \leftarrow 1_{11}, 3_{22} \leftarrow 2_{12}$ lines could be identified, being of similar intensity as the corresponding A0 species. Starting from these assignments, we explicitly searched for the same combination difference loops as those found for the A0 species (see Figure 8). After a sufficient number of lines had been assigned, a separate fit of the E0 species was performed with *spfit* using the same parameters accounting for the ring tunneling motion (E, E_J, F_{ab} , and F_{bc}). In addition, two odd power order parameters, D_a and D_c , as well as their higher-order parameters, D_{aK}, D_{cK}, D_{cJK} , and D_{cKK} [42], are required to fit the E0 state separately, as implemented in the H_{op} operator, as follows:

$$H_{op} = (D_a + D_{aK}J_a^2)J_a + (D_c + D_{cK}J_c^2 + D_{cKK}J_c^4)J_c \quad (6)$$

We achieved an rms deviation of 10.6 kHz for 69 E0 lines. We were confident about the assignments, but due to the low number of lines, no attempts were made to further reduce this deviation by adding more parameters. The fit is shown as Fit E0 in Table S5 of the Supplementary Materials with a list of all fitted frequencies along with their residuals. To access the methyl torsional barrier, the A0 and E0 species lines were input into XIAM. Similar to the case of the A0 species, we obtained an extremely high rms deviation of 6.9 MHz. The V_3 potential was determined to be 136 cm^{-1} . The XIAM fit is given in Table S6 along with the observed-minus-calculated values.

2.2.5. Assignment of the $v_t = 1$, E Species (E1)

The predictive power of Fit A0/A1 and Fit E0 enabled us to exclude all lines belonging to the A0, A1, and E0 species from the recorded scan. It was then possible to identify some E1 species lines corresponding to the most intense E0 lines, which are of similar intensity as those of the A1 species, as shown exemplarily for the $2_{21} \leftarrow 1_{11}$ transitions in Figure 9. Eventually, we found 17 E1 lines and fitted them together with the E0 lines using *spfit*. This fit is given as Fit E0/E1 in Table S5 of the Supplementary Materials. Similar to Fit A0/A1, the rotational and centrifugal distortion constants were fitted separately for the E0 and E1 species. Odd power order parameters are required, as in the case of Fit E0. They are fitted separately for the E0 and E1 species. Due to the low intensity of the E1 lines, we could not close any combination difference loops. Consequently, though we are confident about most of the E1 assignments, conclusive proof is lacking. The fit chosen for Table S5 has an rms deviation of 358.8 kHz, but we had to take out 9 E0 lines with $K_a = 3$. Therefore, this high rms deviation may arise from the limited number of fit parameters. The frequency list is also given in Table S5.

2.2.6. Global Fitting of the A0, E0, A1, E1 Sub-States

We then fit the rotational transition frequencies of all four states, A0, A1, E0, and E1, simultaneously, considering, in principle, all the interactions between the four sublevels of the vibrational ground state. A0 will interact with A1 and E0 via Coriolis and V_3 internal rotation couplings, respectively. Similarly, the other three states interact with two other states. The results of this global fit are reported in Table 1. In the fit, the value of $\Delta E_{A0/E0}$ was fixed at 16 GHz, corresponding to the V_3 barrier determined by XIAM.

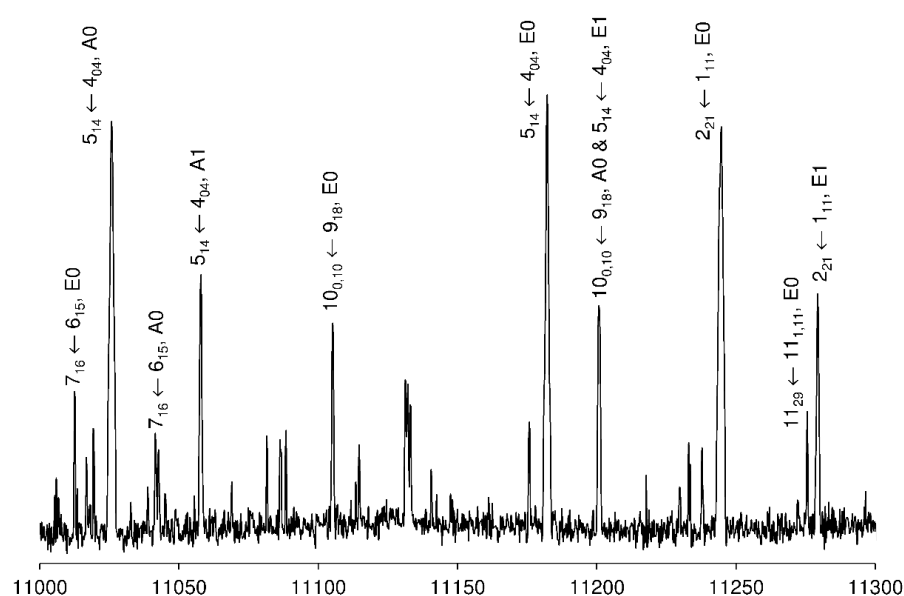


Figure 9. A portion of the scan of phenyl acetate in the frequency range from 11,000 to 11,300 MHz recorded by overlapping spectra with 50 co-added decays per each spectrum. The logarithmic intensities are in arbitrary units. The assigned lines are labeled with the corresponding rotational quantum numbers and tunneling species.

Table 1. Molecular parameters obtained from a simultaneous fitting of the A0, A1, E0 and E1 sub-state lines of phenyl acetate using the program *spfit*.

Par. ^a	Unit	A0	A1	E0	E1
<i>A</i>	MHz	3637.78667(33)	3640.89405(39)	3622.9532(38)	3627.018(13)
<i>B</i>	MHz	803.88947(10)	803.39084(22)	803.80593(60)	803.3164(40)
<i>C</i>	MHz	750.97790(11)	749.94839(46)	750.94959(64)	749.8638(26)
<i>D_J</i>	kHz	0.2243(17)	−0.0429(32)	−1.582(53)	2.99(18)
<i>D_{JK}</i>	kHz	2.3359(92)	2.451(13)	7.78(77)	−35.56(19)
<i>D_K</i>	kHz			0.193(13)	
<i>d₁</i>	kHz	−0.00130(24)	0.0366(18)	0.1360(13)	−
<i>d₂</i>	kHz	0.1583(13)	−0.0142(23)	1.509(48)	−
ΔE	GHz	36.40881(32)		33.533(75)	
<i>F_{bc}</i>	MHz	28.0660(25)		25.07(11)	
<i>F_{bcK}</i>	kHz	0.1877(69)		−0.334(53)	
<i>F_{ab}</i>	MHz	78.5913(19)		76.77(12)	
<i>F_{abJ}</i>	kHz	3.307(47)		0.0139(10)	
<i>F_{abK}</i>	kHz	1.009(14)		0.01385(41)	
<i>D_a</i>	MHz			401.8794(20)	380.792(12)
<i>D_c</i>	MHz			32.6882(22)	36.129(92)
<i>D_{aJ}</i>	MHz			−0.14776(32)	−0.0762(12)
<i>D_{cJ}</i>	MHz			2.376(76)	−8.860(98)
<i>D_{aK}</i>	kHz			7.596(90)	−11.42(27)
<i>D_{cK}</i>	kHz			−7.73(27)	−9.49(97)
<i>N^b</i>			240		
$\sigma/\sigma_{\text{exp}}^{\text{c}}$			1.22		

^a All parameters refer to the principal axis system. Watson's S reduction in F representation was used. ^b Numbers of lines included in the fit. ^c Reduced deviation of the fit when setting the millimeter-wave and microwave measurement errors to 80 kHz and 3 kHz, respectively.

Except for *D_K*, the values of the centrifugal distortion constants are not so homogeneous among the four states. This can be due to the fact that not all the interactions are taken into account. For example, some “local” interactions of rotational states belong to different vibrational sublevels, and their effects can be “included” in the so-called “pseudo-centrifugal distortion constants”, allowing accurate fittings to the experimental uncertainty

of the measured frequencies. The output of the *spfit* program leading to the parameters of Table 1 is reported in Table S7 of the Supplementary Materials. Similar to the case of Fit E0/E1 in Table S5 of the Supplementary Materials, we could not include the 9 E0 lines with $K_a = 3$ and also had to take out 5 E1 lines. We note that a number of $v_t = 0 \longleftrightarrow 1$ interstate μ_a -R-type transitions have been used in the fit, while only μ_b -type interstate transitions should be observed. These “forbidden” transitions originate from an accidental but systematic μ_b -mixing of the $v_t = 0, J_{7,x}$ and the $v_t = 1, J_{6,y}$, which have very similar energies for each J . As an example, for $J = 14$, the energies of the degenerate levels $v_t = 0, 14_{7,7}$, and $14_{7,6}$ are about 303 GHz, being the same as the value of the $v_t = 1, 14_{6,8}$, and $14_{6,7}$ degenerate levels. Their mixing will give a partial μ_b -character to the reported, apparently pure μ_a -type transitions. Moreover, for the E0 and E1 species, about half of the lines are intrastate μ_b -transitions, while due to the kind of motion, only interstate μ_b -transitions are allowed. For the E species, the K_a and K_c quantum numbers have no meaning for those perturbation allowed transitions, because they only indicate the order of energy.

From the value of the parameters D_a or D_c of the E0 state, it is possible to estimate the V_3 barrier to internal rotation of the methyl group when ac represents a molecular plane of symmetry [43–45]. This is not the case of phenyl acetate, but due to the low barrier to inversion at $\alpha = 90^\circ$, the vibrational wavefunctions of $v_t = 0$ are exactly symmetric with respect to the ac plane. In addition, when trying to fit the D_b parameter, it was immediately set to zero. For this reason, we believe that the method to estimate V_3 from D_a (or D_c) is applicable for phenyl acetate [29,43].

We first set a system of the following two equations:

$$D_a = \frac{A}{r} W_{v\sigma}^{(1)} \lambda_a \text{ and} \quad (7)$$

$$D_c = \frac{C}{r} W_{v\sigma}^{(1)} \lambda_c \quad (8)$$

to calculate the first-order perturbation coefficients $W_{0,E}^{(1)}$ [46] through the relations, as follows:

$$W_{0,E}^{(1)} = \frac{D_g}{F\rho_g} \quad \text{with } g = a \text{ or } c, \quad (9)$$

$\lambda_g = \cos(\angle i, g)$, assuming the top inertial defect $I_\alpha = 3.2 \text{ u}\text{\AA}^2$. Since the ac plane can be considered as a symmetry plane ($\angle i, a$) + ($\angle i, c$) = 90° ; therefore, λ_a and λ_c are dependent, leading to only two unknowns. The solution of the two-equation system provides ($\angle i, a$) = 22.1° , ($\angle i, c$) = 67.9° , and $W_{0,E}^{(1)} = 0.1133$.

From the coefficient $W_{0,E}^{(1)}$, the reduced barrier s estimated through Herschbach’s tables is 11.5 [46]. The reduced barrier is related both to the methyl internal rotation barrier

$$V_3 = \frac{9}{4} F \cdot s \quad (10)$$

and the splitting between the A and E levels, as follows:

$$\Delta_0 = \frac{27}{8} F w_1^{v=0} \quad (11)$$

with $w_1^{v=0} = -0.0275$ from Herschbach’s tables. The achieved values are $\Delta_0 = 0.5 \text{ cm}^{-1}$ and thus $V_3 = 143 \text{ cm}^{-1}$.

2.3. Flexible Model Calculations

The experimental value of the $\Delta E_{A0/A1}$ vibrational splitting can be used to determine the small barrier at $\alpha = 90^\circ$. In order to handle a simple expression, we first defined $\tau = \alpha - 90$ and used the following double minimum potential:

$$V(\tau) = B_2[1 - (\tau/\tau_0)^2]^2 \quad (12)$$

where B_2 is the barrier at $\tau = 0^\circ$ and τ_0 is the equilibrium value of the inversion angle. Such an equation is suitable to describe our potential energy function in a small interval that includes the two minima and the “transition state”. The energies and wavefunctions of vibrational states related to the skeletal torsion were calculated numerically with a suitable model [47]. We fixed the parameter τ_0 to the *ab initio* value, calculated B_2 , and applied Meyer’s one-dimensional numerical flexible model [47]. The value $\Delta E_{A0/A1} = 36.4$ GHz was reproduced when B_2 was set to 68 cm^{-1} . In the flexible model calculation, the τ coordinate has been considered in the $\pm 50^\circ$ range and solved into 41 mesh points [47]. This range is expected to reproduce the low energy part of the potential energy curve of this motion, describing the minima and the barrier at the perpendicular configuration. The value of $B_2 = 68 \text{ cm}^{-1}$ is considerably higher than the value obtained by the Hamiltonian in Equation (1). This discrepancy can be due to the fact that, with the numerical method, the value of the reduced constant of the motion F is calculated for every point, and it undergoes significant variations in the considered range.

3. Discussion

The A and E species lines belonging to the $v_t = 0$ tunneling species of phenyl acetate were assigned. The initial assignments of both species are secured by an extensive interlocking network of combination difference loops. These A0 and E0 states could be fitted separately using the *spfit* program to rms deviations close to the measurement accuracy if parameters accounting for the ring tunneling motion are considered (see Tables S4 and S5 of the Supplementary Materials). This “local” approach has been proven to be very powerful as assignment guidance in many previous studies where methyl internal rotations with low torsional barriers are present [42,48–51].

Though it is possible to derive the value of the barrier to internal rotation from the fitted odd power parameters D_a and D_c , the obtained barrier ($V_3 = 143 \text{ cm}^{-1}$) might not be so accurate due to several approximations [29]. The V_3 barrier was also deduced by a XIAM fit, including the A0/E0 species. Since XIAM does not take into account the interactions of A0 and E0 with A1 and E1, the standard deviation of the fit is terribly high. However, the value of $V_3 = 136 \text{ cm}^{-1}$ obtained from this fit is extremely close to the value of $135.3498(38) \text{ cm}^{-1}$ found for isopropenyl acetate, where the isopropenyl group is also tilted out of the O-(C=O)-C plane by an angle of about 70° [14]. As summarized in a review by Nguyen and Kleiner [52], a torsional barrier of the acetyl methyl group $\text{CH}_3\text{-COO}$ is almost invariant at 100 cm^{-1} for α,β -saturated acetates [5–10]. In α,β -unsaturated acetates with the two current representatives vinyl acetate [11,12] and two isomers of butadienyl acetate [13], the conjugation over the double bond(s) increases the barrier height to 150 cm^{-1} . In both isopropenyl acetate and phenyl acetate, the double bond is not located in the O-(C=O)-C plane, leading to a less effective conjugation. The torsional barrier of about 136 cm^{-1} , between 100 cm^{-1} and 150 cm^{-1} , reflects well this observation.

The $v_t = 1$ spectrum is significantly less intense than the $v_t = 0$ one (see Figure 9, for example, note that the intensity is on a logarithmic scale to better visualize the weaker A1 and E1 species lines). The number of line ratio is $N_1/N_0 \approx 1/4$. The tunneling ΔE parameter could be determined and has a value of 36.4 GHz for the A0/A1 and 33.5 for the E0/E1 fit (see Table 1). Both values are close to the value of 30.6 GHz obtained from calculations using a simple two-top torsional Hamiltonian of the $\text{CH}_3\text{-COO}$ group and the phenyl ring. Compared to phenyl formate [25], where the ring tunneling is respected to an H-COO frame instead of the heavier $\text{CH}_3\text{-COO}$ frame as in the case of phenyl acetate,

the Coriolis splitting ΔE_{01} of 46.2231(25) GHz of the former is significantly larger. On the other hand, the $\Delta E_{A0/A1}$ value of phenyl acetate is an order of magnitude larger than the value of 3.732027(43) GHz in *E*-phenylformamide [24]. The smaller tilt angle of 40° of the phenyl ring out of the (NH)(CO) plane in *E*-phenylformamide is mainly responsible for this Coriolis splitting being drastically lower than in phenyl formate or phenyl acetate.

The coupled LAMs observed in the microwave spectrum of phenyl acetate are very similar to those found in pinacolone [41], where in the latter molecule, a methyl internal rotation is coupled with the tunneling motion of the *tert*-butyl group. We show here that a model, often successful, as implemented in *XIAM*, fails in some specific cases. Even a very powerful and flexible program such as *spfit/spcat* encounters problems when tunneling motions between a double minimum potential come into play with a low-barrier methyl torsion. Kleiner's BELGI-hybrid program may be suitable to treat this problem in another global approach, taking into account the interactions of all four sub-states [53]. After the A0, A1, E0, and E1 species were assigned, all lines remaining in the broadband scan are of weak intensity and are neglected.

Supplementary Materials: The following are available online at <https://www.mdpi.com/article/10.3390/molecules27092730/s1>, Table S1: Fourier expansion of the potential energy curve of phenyl acetate given in Figures 3 and 4, Table S2: Nuclear coordinates in the principal inertial axes of conformer I_b shown in Figure 2, Table S3: Fourier coefficients of the 2D-PES shown in Figure 5, Table S4: Fitted molecular parameters of the A1 and A2 state lines using *spfit* and the frequency list, Table S5: Fitted molecular parameters of the E1 and E2 state lines using *spfit* and the frequency list, Table S6: Fitted molecular parameters of the A0 and E0 state lines using *XIAM* and the frequency list, Table S7: Frequency list of the fit given in Table 1.

Author Contributions: Conceptualization, W.C. and W.S.; methodology, W.C., W.S. and H.V.L.N.; validation, L.E., A.M., S.M., W.C. and H.V.L.N.; formal analysis, L.F., L.E., A.M., S.M., W.C., W.S. and H.V.L.N.; investigation, L.F., L.E., A.M., S.M., W.C., W.S. and H.V.L.N.; resources, A.M., S.M., W.C., W.S. and H.V.L.N.; data curation, L.F., L.E., A.M., S.M., W.C., W.S. and H.V.L.N.; writing—original draft preparation, L.F. and H.V.L.N.; writing—review and editing, L.E., A.M., S.M., W.C. and H.V.L.N.; visualization, L.F. and H.V.L.N.; supervision, A.M., S.M., W.C., W.S. and H.V.L.N.; project administration, H.V.L.N.; funding acquisition, A.M., S.M., W.C., W.S. and H.V.L.N. All authors have read and agreed to the published version of the manuscript.

Funding: This research was funded by the Agence Nationale de la Recherche ANR, grant number ANR-18-CE29-0011, by the Italian MIUR PRIN, project number 2010ERFKXL_001, and by the University of Bologna (RFO). Simulations were performed with computing resources granted by the RWTH Aachen University under the project rwth0506.

Institutional Review Board Statement: Not applicable.

Informed Consent Statement: Not applicable.

Data Availability Statement: Data are contained within the article and Supplementary Materials.

Conflicts of Interest: The authors declare no conflict of interest.

References

1. Rajabi, F.; Luque, R. Solventless Acetylation of Alcohols and Phenols Catalyzed by Supported Iron Oxide Nanoparticles. *Catal. Commun.* **2014**, *45*, 129–132. [[CrossRef](#)]
2. González-Núñez, M.E.; Mello, R.; Olmos, A.; Asensio, G. Baeyer–Villiger Oxidation with Potassium Peroxomonosulfate Supported on Acidic Silica Gel. *J. Org. Chem.* **2005**, *70*, 10879–10882. [[CrossRef](#)] [[PubMed](#)]
3. Seo, S.; Taylor, J.B.; Greaney, M.F. Protodecarboxylation of Benzoic Acids under Radical Conditions. *Chem. Commun.* **2012**, *48*, 8270–8272. [[CrossRef](#)] [[PubMed](#)]
4. Samid, D.; Shack, S.; Sherman, L.T. Phenylacetate: A Novel Nontoxic Inducer of Tumor Cell Differentiation. *Cancer Res.* **1992**, *52*, 1988–1992. [[PubMed](#)]
5. Nguyen, H.V.L.; Kleiner, I.; Shipman, S.T.; Mae, Y.; Hirose, K.; Hatanaka, S.; Kobayashi, K. Extension of the Measurement, Assignment, and Fit of the Rotational Spectrum of the Two-Top Molecule Methyl Acetate. *J. Mol. Spectrosc.* **2014**, *299*, 17–21. [[CrossRef](#)]

6. Jelisivac, D.; Cortés-Gómez, D.C.; Nguyen, H.V.L.; Sutikdja, L.W.; Stahl, W.; Kleiner, I. The Microwave Spectrum of the Trans Conformer of Ethyl Acetate. *J. Mol. Spectrosc.* **2009**, *257*, 111. [[CrossRef](#)]
7. Sutikdja, L.W.; Stahl, W.; Sironneau, V.; Nguyen, H.V.L.; Kleiner, I. Structure and Internal Dynamics of *n*-Propyl Acetate Studied by Microwave Spectroscopy and Quantum Chemistry. *Chem. Phys. Lett.* **2016**, *663*, 145–149. [[CrossRef](#)]
8. Attig, T.; Sutikdja, L.W.; Kannengießler, R.; Kleiner, I.; Stahl, W. The Microwave Spectrum of *n*-Butyl Acetate. *J. Mol. Spectrosc.* **2013**, *284–285*, 8–15. [[CrossRef](#)]
9. Attig, T.; Kannengießler, R.; Kleiner, I.; Stahl, W. Conformational Analysis of *n*-Pentyl Acetate Using Microwave Spectroscopy. *J. Mol. Spectrosc.* **2013**, *290*, 24–30. [[CrossRef](#)]
10. Attig, T.; Kannengießler, R.; Kleiner, I.; Stahl, W. The Microwave Spectrum of *n*-Hexyl Acetate and Structural Aspects of *n*-Alkyl Acetates. *J. Mol. Spectrosc.* **2014**, *298*, 47. [[CrossRef](#)]
11. Velino, B.; Maris, A.; Melandri, S.; Caminati, W. Millimeter Wave Free-Jet Spectrum of Vinyl Acetate. *J. Mol. Spectrosc.* **2009**, *256*, 228–231. [[CrossRef](#)]
12. Nguyen, H.V.L.; Jabri, A.; Van, V.; Stahl, W. Methyl Internal Rotation in the Microwave Spectrum of Vinyl Acetate. *J. Phys. Chem. A* **2014**, *118*, 12130–12136. [[CrossRef](#)] [[PubMed](#)]
13. Jabri, A.; Van, V.; Nguyen, H.V.L.; Stahl, W.; Kleiner, I. Probing the Methyl Torsional Barriers of the E and Z Isomers of Butadienyl Acetate by Microwave Spectroscopy. *ChemPhysChem* **2016**, *17*, 2660–2665. [[CrossRef](#)] [[PubMed](#)]
14. Nguyen, H.V.L.; Stahl, W. The Microwave Spectrum of Isopropenyl Acetate: An Asymmetric Molecule with Two Internal Rotors. *J. Mol. Spectrosc.* **2010**, *264*, 120–124. [[CrossRef](#)]
15. Reinhold, B.; Finneran, I.A.; Shipman, S.T. Room Temperature Chirped-Pulse Fourier Transform Microwave Spectroscopy of Anisole. *J. Mol. Spectrosc.* **2011**, *270*, 89–97. [[CrossRef](#)]
16. Ferres, L.; Stahl, W.; Nguyen, H.V.L. The Molecular Structure of Phenetole Studied by Microwave Spectroscopy and Quantum Chemical Calculations. *Mol. Phys.* **2016**, *114*, 2788–2793. [[CrossRef](#)]
17. Melandri, S.; Giuliano, B.M.; Maris, A.; Favero, L.B.; Ottaviani, P.; Velino, B.; Caminati, W. Methylsalicylate: A Rotational Spectroscopy Study. *J. Phys. Chem. A* **2007**, *111*, 9076–9079. [[CrossRef](#)]
18. Lei, J.; Zhang, J.; Feng, G.; Grabow, J.-U.; Gou, Q. Conformational Preference Determined by Inequivalent n-Pairs: Rotational Studies on Acetophenone and its Monohydrate. *Phys. Chem. Chem. Phys.* **2019**, *21*, 22888–22894. [[CrossRef](#)]
19. Utzat, K.A.; Bohn, R.K.; Montgomery, J.A., Jr.; Michels, H.H.; Caminati, W. Rotational Spectrum, Tunneling Motions, and Potential Barriers of Benzyl Alcohol. *J. Phys. Chem. A* **2010**, *114*, 6913–6916. [[CrossRef](#)]
20. Evangelisti, L.; Caminati, W. Modeling the Internal Rotation Tunneling in Benzyl Alcohol by Ring Fluorination: The Rotational Spectrum of 3,5-Difluorobenzyl Alcohol. *Chem. Phys. Lett.* **2019**, *737S*, 100004. [[CrossRef](#)]
21. Godfrey, P.D.; Hatherley, L.D.; Brown, R.D. The Shapes of Neurotransmitters by Millimeter-Wave Spectroscopy: 2-Phenylethylamine. *J. Am. Chem. Soc.* **1995**, *117*, 8204. [[CrossRef](#)]
22. López, J.C.; Cortijo, V.; Blanco, S.; Alonso, J.L. Conformational Study of 2-Phenylethylamine by Molecular-Beam Fourier Transform Microwave Spectroscopy. *Phys. Chem. Chem. Phys.* **2007**, *9*, 4521–4527. [[CrossRef](#)] [[PubMed](#)]
23. Cabezas, C.; Varela, M.; Caminati, W.; Mata, S.; López, J.C.; Alonso, J.L. The Two Conformers of Acetanilide Unraveled Using LA-MB-FTMW Spectroscopy. *J. Mol. Spectrosc.* **2011**, *268*, 42–46. [[CrossRef](#)]
24. Aviles Moreno, J.-R.; Petitprez, D.; Huet, T.R. The Conformational Flexibility in N-Phenylformamide: An Ab Initio Approach Supported by Microwave Spectroscopy. *Chem. Phys. Lett.* **2006**, *419*, 411–416. [[CrossRef](#)]
25. Ferres, L.; Mouhib, H.; Stahl, W.; Schwell, M.; Nguyen, H.V.L. Molecular Structure and Ring Tunneling of Phenyl Formate as Observed by Microwave Spectroscopy and Quantum Chemistry. *J. Mol. Spectrosc.* **2017**, *337*, 59–64. [[CrossRef](#)]
26. Cleeton, C.E.; Williams, N.H. Electromagnetic Waves of 1.1 cm Wave-Length and the Absorption Spectrum of Ammonia. *Phys. Rev.* **1934**, *45*, 234. [[CrossRef](#)]
27. Nguyen, H.V.L.; Gulaczyk, I.; Kreglewski, M.; Kleiner, I. Large Amplitude Inversion Tunneling Motion in Ammonia, Methylamine, Hydrazine, and Secondary Amines: From Structure Determination to Coordination Chemistry. *Coord. Chem. Rev.* **2021**, *436*, 213797. [[CrossRef](#)]
28. Pickett, H.M. The Fitting and Prediction of Vibration-Rotation Spectra with Spin Interactions. *J. Mol. Spectrosc.* **1991**, *148*, 371–377. [[CrossRef](#)]
29. Herbers, S.; Zingsheim, O.; Nguyen, H.V.L.; Bonah, L.; Heyne, B.; Wehres, N.; Schlemmer, S. Internal Rotation Arena: Program Performances on the Low Barrier Problem of 4-Methylacetophenone. *J. Chem. Phys.* **2021**, *155*, 224302. [[CrossRef](#)]
30. Hartwig, H.; Dreizler, H. The Microwave Spectrum of trans-2,3-Dimethyloxirane in Torsional Excited States. *Z. Naturforsch.* **1996**, *51a*, 923–932. [[CrossRef](#)]
31. Frisch, M.J.; Trucks, G.W.; Schlegel, H.B.; Scuseria, G.E.; Robb, M.A.; Cheeseman, J.R.; Scalmani, G.; Barone, V.; Petersson, G.A.; Nakatsuji, H.; et al. Gaussian 16, Revision B.01. Gaussian Inc.: Wallingford, CT, USA, 2016.
32. Moran, D.; Simmonett, A.C.; Leach, F.E.; Allen, W.D.; Schleyer, P.v.R.; Schaefer, H.F. Popular Theoretical Methods Predict Benzene and Arenes To Be Nonplanar. *J. Am. Chem. Soc.* **2006**, *128*, 9342–9343. [[CrossRef](#)] [[PubMed](#)]
33. Schlegel, H.B. Optimization of Equilibrium Geometries and Transition Structures. *J. Comput. Chem.* **1982**, *3*, 214–218. [[CrossRef](#)]
34. Melandri, S.; Caminati, W.; Favero, L.B.; Millemaggi, A.; Favero, P.G. A Microwave Free Jet Absorption Spectrometer and its First Applications. *J. Mol. Struct.* **1995**, *352–353*, 253–258. [[CrossRef](#)]

35. Melandri, S.; Maccaferri, G.; Maris, A.; Millemaggi, A.; Caminati, W.; Favero, P.G. Observation of the Rotational Spectra of van der Waals Complexes by Free Jet Absorption Millimeter Wave Spectroscopy: Pyridine-Argon. *Chem. Phys. Lett.* **1996**, *261*, 267–271. [[CrossRef](#)]
36. Calabrese, C.; Maris, A.; Evangelisti, L.; Favero, L.B.; Melandri, S.; Caminati, W. Keto–Enol Tautomerism and Conformational Landscape of 1,3-Cyclohexanedione from Its Free Jet Millimeter-Wave Absorption Spectrum. *J. Phys. Chem. A* **2013**, *117*, 13712–13718. [[CrossRef](#)]
37. Evangelisti, L.; Maris, A.; Melandri, S.; Caminati, W. *Internal Dynamics in Phenylacetate*, Poster communication D42, 22nd ed.; International Conference on High Resolution Molecular Spectroscopy: Praha, Czech Republic, 2012.
38. Caminati, W.; Millemaggi, A.; Alonso, J.L.; Lesarri, A.; Lopez, J.C.; Mata, S. Molecular Beam Fourier Transform Microwave Spectrum of the Dimethylether–Xenon Complex: Tunnelling Splitting and ^{131}Xe Quadrupole Coupling Constants. *Chem. Phys. Lett.* **2004**, *392*, 1–6. [[CrossRef](#)]
39. Grabow, J.-U.; Stahl, W.; Dreizler, H. A Multioctave Coaxially Oriented Beam-resonator Arrangement Fourier-Transform Microwave Spectrometer. *Rev. Sci Instrum.* **1996**, *67*, 4072–4084. [[CrossRef](#)]
40. Grabow, J.-U.; Stahl, W. A Pulsed Molecular Beam Microwave Fourier Transform Spectrometer with Parallel Molecular Beam and Resonator Axes. *Z. Naturforsch.* **1990**, *45a*, 1043–1044. [[CrossRef](#)]
41. Zhao, Y.; Nguyen, H.V.L.; Stahl, W.; Hougen, J.T. Unusual Internal Rotation Coupling in the Microwave Spectrum of Pinacolone. *J. Mol. Spectrosc.* **2015**, *318*, 91–100. [[CrossRef](#)]
42. Herbers, S.; Fritz, S.M.; Mishra, P.; Nguyen, H.V.L.; Zwier, T.S. Local and Global Approaches to Treat the Torsional Barriers of 4-Methylacetophenone Using Microwave Spectroscopy. *J. Chem. Phys.* **2020**, *152*, 074301. [[CrossRef](#)]
43. Evangelisti, L.; Favero, L.B.; Maris, A.; Melandri, S.; Vega-Toribio, A.; Lesarri, A.; Caminati, W. Rotational Spectrum of Trifluoroacetone. *J. Mol. Spectrosc.* **2010**, *259*, 65–69. [[CrossRef](#)]
44. Maris, A.; Calabrese, C.; Favero, L.B.; Evangelisti, L.; Usabiaga, I.; Mariotti, S.; Codella, C.; Podio, L.; Balucani, N.; Ceccarelli, C.; et al. Laboratory Measurements and Astronomical Search for Thioacetamide. *ACS Earth Space Chem.* **2019**, *21*, 1537–1549. [[CrossRef](#)]
45. Maris, A.; Melandri, S.; Evangelisti, L.; Vigorito, A.; Sigismondi, S.; Calabrese, C.; Usabiaga, I. Structure and Dynamics of Methacrylamide, a Computational and Free-Jet Rotational Spectroscopic Study. *J. Mol. Struct.* **2022**, *1248*, 131391. [[CrossRef](#)]
46. Herschbach, D.R. Tables of Mathieu Integrals for the Internal Rotation Problem. *J. Chem. Phys.* **1957**, *27*, 975. [[CrossRef](#)]
47. Meyer, R. Flexible Models for Intramolecular Motion, a Versatile Treatment and its Application to Glyoxal. *J. Mol. Spectrosc.* **1979**, *76*, 266–300. [[CrossRef](#)]
48. Ohashi, N.; Hougen, J.T.; Suenram, R.; Lovas, F.J.; Kawashima, Y.; Fujitake, M.; Pyka, J. Analysis and Fit of the Fourier-Transform Microwave Spectrum of the Two-Top Molecule *N*-Methylacetamide. *J. Mol. Spectrosc.* **2004**, *227*, 28–42. [[CrossRef](#)]
49. Mélan, J.; Khemissi, S.; Nguyen, H.V.L. Steric Effects on Two Inequivalent Methyl Internal Rotations of 3,4-Dimethylfluorobenzene. *Spectrochim. Acta A* **2021**, *253*, 119564. [[CrossRef](#)]
50. Khemissi, S.; Pérez Salvador, A.; Nguyen, H.V.L. Large Amplitude Motions in 2,3-Dimethylfluorobenzene: Steric Effects Failing to Interpret Hindered Methyl Torsion. *J. Phys. Chem. A* **2021**, *125*, 8542–8548. [[CrossRef](#)]
51. Nguyen, T.; Stahl, W.; Nguyen, H.V.L.; Kleiner, I. Local Versus Global Approaches to Treat Two Equivalent Methyl Internal Rotations and ^{14}N Nuclear Quadrupole Coupling of 2,5-Dimethylpyrrole. *J. Chem. Phys.* **2021**, *154*, 204304. [[CrossRef](#)]
52. Nguyen, H.V.L.; Kleiner, I. Understanding (Coupled) Large Amplitude Motions: The Interplay of Microwave Spectroscopy, Spectral Modeling, and Quantum Chemistry. *Phys. Sci. Rev.* **2020**, 20200037. [[CrossRef](#)]
53. Kleiner, I.; Hougen, J.T. A Hybrid Program for Fitting Rotationally Resolved Spectra of Floppy Molecules with One Large-Amplitude Rotatory Motion and One Large-Amplitude Oscillatory Motion. *J. Phys. Chem. A* **2015**, *119*, 10664–10676. [[CrossRef](#)] [[PubMed](#)]